MATERIALS SCIENCE

Functional soft materials from blue phase liquid crystals

Kushal Bagchi[1], Tadej Emeršič[1], José A. Martínez-González[2], Juan J. de Pablo[1,3]*, Paul F. Nealey[1,3]*

Blue phase (BP) liquid crystals are chiral fluids wherein millions of molecules self-assemble into cubic lattices that are on the order of hundred nanometers. As the unit cell sizes of BPs are comparable to the wavelength of light, they exhibit selective Bragg reflections in the visible. The exploitation of the photonic properties of BPs for technological applications is made possible through photopolymerization, a process that renders mechanical robustness and thermal stability. We review here the preparation and characterization of stimuli-responsive, polymeric photonic crystals based on BPs. We highlight recent studies that demonstrate the promise that polymerized BP photonic crystals hold for colorimetric sensing and dynamic light control. We review using Landau–de Gennes simulations for predicting the self-assembly of BPs and the potential for using theory to guide experimental design. Finally, opportunities for using BPs to synthesize new soft materials, such as highly structured polymer meshes, are discussed.

INTRODUCTION

Chirality plays a profound role on the physics of liquid crystals (LCs). Imparting chirality to LCs results in mesophases that exhibit unique material properties. The chiral smectic phase, SmC*, exhibits ferroelectricity, a property usually seen only in solids and one that has been exploited to prepare fast switching microdisplays. Doping a chiral molecule into an achiral nematic matrix leads to the formation of the cholesteric phase. Molecules in the cholesteric phase are organized into helical structures that exhibit Bragg reflections (*1*); imparting chirality to the nematic phase therefore enables preparation of liquid photonic crystals. Cholesteric structures are observed in living systems (*2*) where they perform diverse roles from giving rise to structural coloration in insects (*3*, *4*) to improving the mechanical properties of plant cell walls (*5*). In systems with a high degree of chirality, three-dimensional photonic crystals called blue phases (BPs) are formed, wherein millions of molecules organize into cubic lattices that typically range in size from 100 to 400 nm (*6*, *7*). BPs are testament to the complex and novel structures that can occur through spontaneous self-assembly in chiral systems.

BPs exhibit hierarchical structure. As shown in Fig. 1A, doping a chiral molecule into a nematic matrix leads to helical twisting, with the screw axis of the helix perpendicular to the long axis of the mesogens. The length over which the mesogens execute a rotation of 360° is known as the pitch, *p*. At high concentrations of the chiral dopant, twisting can occur in orthogonal directions, leading to the formation of double-twist cylinders (DTCs). The molecular orientation within DTCs is shown in Fig. 1A. From one edge of the cylinder to the other, the molecules rotate 90° or *p*/4. The twisting in DTCs is similar to that seen in cholesterics; however, it occurs along two directions rather than one in DTCs. The size of DTCs is usually of the order of 100 nm. In BPs, DTCs organize into cubic lattices. As cylinders cannot continuously fill space, the void between DTCs is occupied by high energy defect regions known as disclinations. The size of disclinations is usually of the order of 10 nm. The molecular orientation in the disclination region is believed to be isotropic (*8*). Figure 1B illustrates the two ordered structures seen in BPs, namely, the body-centered cubic (BCC) BPI and simple cubic (SC) BPII. An amorphous BP, BPIII, also exists, which we shall not discuss here. We direct the interested reader to referenced articles that delve into BPIII in depth (*9*, *10*). The BP structure bears resemblance to that of magnetic skyrmions; BPI and BPII can be regarded as phases of fractional skyrmions and singular disclination lines (*11*, *12*).

BPs occur in a narrow temperature window between the cholesteric and isotropic phases. The phase diagram of a BP-forming material consisting of a racemic-chiral mixture of mesogen CE5 is shown in Fig. 1C (*13*). BPs occur in that part of the phase diagram where the helical pitch of the chiral fluid is <500 nm. The phase diagram shows that the different BPs (BPI, BPII, and BPIII) are all stable across a temperature window of <1°C. An extensive body of research has been performed to stabilize BPs, a portion of which is reviewed in the next section. The most common strategy to render thermal stability is through photopolymerization, which transfers BP order to solid-like states.

The BP lattice size is comparable to the wavelength of visible light, and BPs therefore are three-dimensional photonic crystals. The size of the BP unit cell determines the wavelength of reflected light. The relationship between the reflected wavelength, λ, and unit cell size, *a*, of BPs is described by the relationship:

$$\lambda = \frac{2na}{\sqrt{(h^2 + k^2 + l^2)}} \quad (1)$$

where *n* is the refractive index and (*hkl*) are the Miller indices describing the lattice orientation of the BP. Contrary to what the name suggests, BPs can reflect light anywhere in the visible and, as Fig. 2A shows, can exhibit any color from blue to red (*14*). Moreover, they can also reflect light outside the visible spectrum.

BP-based photonic crystals are easily tunable and can be prepared from facile fabrication routes. A photograph of three polymerized BPs held with tweezers, along with their reflection spectra, is shown in Fig. 2A (*14*). The three samples with different colors are obtained simply by changing the concentration of the chiral dopant, with the blue and red samples having the highest

[1]Pritzker School of Molecular Engineering, The University of Chicago, Chicago, IL 60637, USA. [2]Facultad de Ciencias, Universidad Autónoma de San Luis Potosí, Av. Parque Chapultepec 1570, San Luis Potosí 78210 SLP, Mexico. [3]Materials Science Division, Argonne National Laboratory, Lemont, IL 60439, USA.
*Corresponding author. Email: depablo@uchicago.edu (J.J.d.P.); nealey@uchicago.edu (P.F.N.)

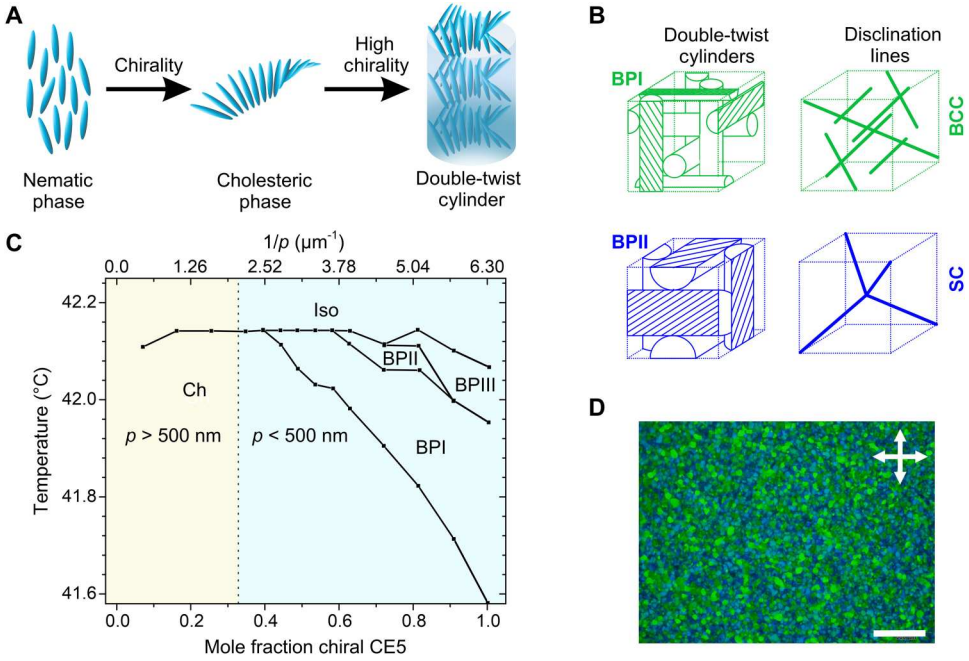

Fig. 1. Structure, phase behavior, and morphology of BP LCs. (**A**) Organization of molecules in nematic and cholesteric phases and within DTCs. (**B**) Organization of DTCs and disclination defects in BPI and BPII into BCC and SC lattices, respectively. (**C**) Composition-temperature phase diagram for chiral-racemic mixtures of CE5; BPs are observed when the pitch, $p < 500$ nm. The region of the phase diagram where BPs are observed is shaded light blue. Adapted with permission from (*13*). Copyright 1987 American Physical Society. (**D**) Representative POM image of a BP LC. The BP sample exhibits polycrystalline morphology. Scale bar, 200 μm.

and lowest concentration of the chiral species, respectively. The preparation of inorganic photonic crystals involves complex and expensive processes such as direct laser writing (*15*) and holographic lithography (*16*). BP-based photonic crystals, in contrast, are prepared from blending organic molecules together and holding the system at the appropriate temperature. We discuss the principles of BP formulation in the following section.

BPs tend to be polycrystalline. A typical polarized optical microscopy (POM) image of a BP LC is shown in Fig. 1D. The different colors in the POM image correspond to different lattice orientations or phases, which according to Eq. 1 reflect light at different wavelengths. Creating BPs with uniform lattice orientation has been an enduring endeavor in the LC community, partly because lattice-aligned BPs exhibit superior performance compared to polycrystals in LC display (LCD) devices (*17*). The "Control of lattice orientation in BPs" section summarizes the different approaches used to form single-crystalline BPs.

BP LCs can respond to electrical stimuli in submillisecond timescales. The response of a polymerized BP to an applied voltage of ≈60 V is shown in Fig. 2B; the polymerized BP exhibits a response time of 100 μs. The application of an electric field distorts the BP structure, causing a change in the intensity of transmitted light. An electric field (E) induces a birefringence (Δn) in BP LCs, which usually scales as E^2. The field-induced birefringence or the Kerr effect forms the basis of a large fraction of BP-based LCDs. In the absence of an electric field and at wavelengths outside the photonic bandgap, BPs are optically isotropic and therefore no light is transmitted between cross-polarizers [BPLCDs operating on the Kerr effect use BPs that reflect in the ultraviolet (UV)]. The field-induced birefringence induces a change in transmitted light intensity in a cross-polarized optical configuration. Samsung has demonstrated a prototype LCD using BPs (*18*).

BPs can be used in reflective displays. The working principle of a reflective display based on polymerized BPs is shown in Fig. 2C. In the absence of a voltage, the device reflects light and is in the on state; the application of an electric field, E, destroys the photonic bandgap, creating the off state of the device. Despite several advantages, such as fast response times, both reflection- and transmission-based BPLCDs suffer from large operating voltages. Reducing the operating voltages of BPLCDs is an enduring endeavor, and we direct the interested reader to the referenced articles, which discuss recent progress in the field (*19*, *20*).

BPs respond to stimuli by changing color and are therefore compelling materials for colorimetric sensors (*21*, *22*). A toluene sensor based on the response of a polymerized BP is shown in Fig. 2D. The polymerized BP provides greater sensitivity to the analyte than the cholesteric and nematic phases. We discuss the potential for BP-based sensors in more detail in the "Stimuli-responsive photonic crystals" section. Although we do not discuss it in detail here, BPs are also of interest for lasing applications (*23*–*26*). A characteristic feature of lasing in BPs is the emission of circularly polarized light (*25*); the handedness of light is determined by that of the chiral dopant. BP lasers are also tunable (*27*); Choi and coworkers (*27*) have varied the laser emission wavelength by more than 50 nm for a single BP material by simply changing the temperature. The tunable nature of BP lasing arises from the tunability of its lattice size.

We review here recent progress in using BPs to fabricate functional soft materials. Progress in making new materials is intimately linked with the chemistry of the BP-forming mixture, and we therefore start with a brief overview of different types of formulations.

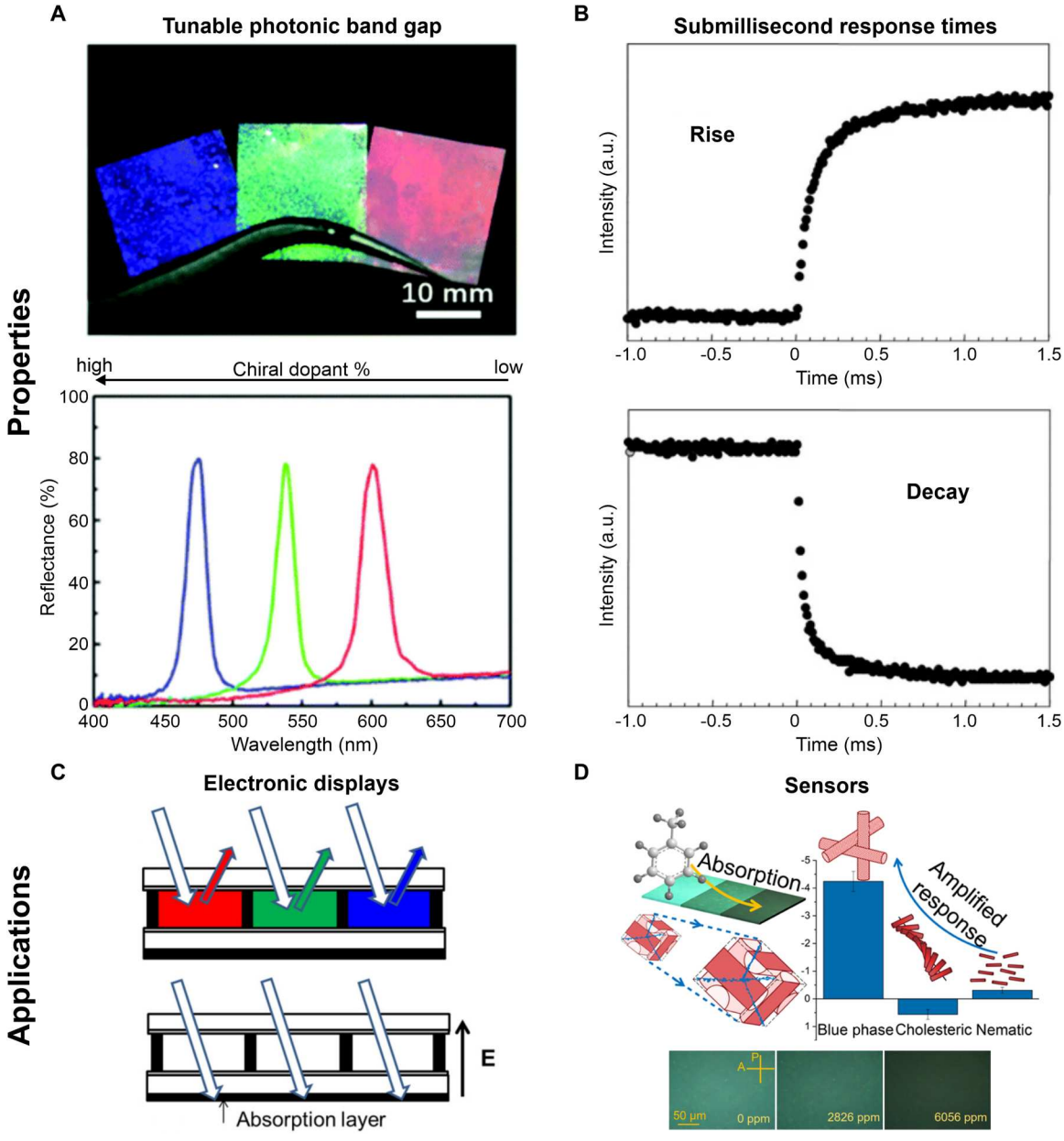

Fig. 2. Properties and applications of polymerized BP LCs. (**A**) Photograph of polymerized BPs and reflection spectroscopy of samples shown above. The color of BPs arises from selective Bragg reflection of visible light and can be tuned by changing the concentration of the chiral dopant. Reproduced with permission from (*14*). Copyright 2019 The Royal Society of Chemistry. (**B**) Transmitted light intensity as a function of time for an LC cell consisting of a polymerized BP sample sandwiched between electrodes. The change in intensity is monitored on the application (rise) and removal (decay) of a voltage of ≈60 V. Intensity changes occur on submillisecond timescales. Reproduced with permission from (*47*). Copyright 2002 Nature Publishing Group. Use of polymerized BPs in (**C**) reflective electronic displays. Reproduced with permission from (*49*). Copyright 2013 American Institute of Physics. Use of polymerized BP LCs in (**D**) colorimetric toluene sensors. Reproduced with permission from (*22*). Copyright 2020 American Chemical Society.

This is followed by a discussion of the preparation of mechanically robust and stimuli-responsive photonic crystals through photopolymerization of low–molecular weight BPs. We then examine the different strategies that have been used to prepare single crystals and elaborate on how these approaches can be used to improve the spatial homogeneity of materials derived from BP LCs. We elaborate on the use of computer simulations to predict the behavior of BPs and guide experimental design. We discuss progress in BP-nanoparticle composites from both theoretical and experimental standpoints. Finally, we identify challenges and interesting directions related to fundamental understanding and technological applications of BPs.

CHEMISTRY OF BP-FORMING MATERIALS

The chemical composition of a BP-forming material plays an important role in determining its structure. The lattice size of a BP, which determines the color it exhibits, depends on the pitch of the chiral system, which in turn depends on the relative concentration of the nematic and chiral molecules. The lattice sizes of BPI and BPII are approximately equal to pitch length and half of the pitch length, respectively. The pitch (p) of a chiral mixture, and consequently the lattice sizes of the different BPs, depends on the concentration of the chiral dopant (c) and its helical twisting power (HTP)

$$p \approx \frac{1}{\mathrm{HTP} \times c} \approx a_{\mathrm{BPI}} \approx 2a_{\mathrm{BPII}} \quad (2)$$

where a_{BPI} and a_{BPII} are the unit cell sizes of BPI and BPII, respectively (*28*). While Eq. 2 is useful for approximating the pitch, it is an inexact relationship. Equation 2 fails to account for the temperature dependence of the helical pitch. The pitch decreases with increasing temperature; in some cases, a 10°C increase in temperature can reduce the chiral pitch by 0.5 μm (*29*).

The composition of a BP-forming material determines its phase behavior. Figure 1C depicts the influence of the concentration of the chiral dopant on the temperature window over which BPI, BPII, and BPIII form. A range of strategies has been used to broaden the temperature window over which liquid BPs occur, such as the use of hydrogen bonding (*30*), dimeric (*31*), biaxial (*32*), and bent-core (*33*, *34*) molecules in the BP-forming mixture. A common approach to widen the BP temperature window is preparing mixtures of molecules with rod-like and non–rod-like shapes. For instance, addition of bent-core mesogens to chiral LC mixtures can widen the temperature window over which BPs form to about ~30°C (*33*). Yang and coworkers (*32*) have recently discovered mixtures consisting of rod-like uniaxial and dimeric biaxial molecules wherein the BP is stable for over 100°C.

The temperature window over which a given BP is stable depends on the interfacial tension, σ, between the disclinations and DTCs. σ is approximated to be the interfacial tension between the host molecules that occupy the DTCs and the dopant molecules that are assumed to segregate to the disclinations. Under this approximation, Fukuda (*35*) used Landau–de Gennes (LdG) theory to estimate that when interfacial tension is around 10^{-5} J/m^2, less than 10% volume fraction of additive is required to stabilize BPI for tens of kelvins. Quantitative measurements of interfacial tension between components could guide the rational design of thermally stable BP formulations.

The composition of a BP-forming material determines the physical states that its structure can be transferred to. Figure 3 shows examples of the different types of BP-forming materials that are commonly studied. Figure 3A shows the simplest composition, consisting of nematic LC former 6OCB and chiral dopant CB15; for this mixture, only the liquid BP state can be accessed (*36*). Figure 3B shows a formulation where a small percentage of the low–molecular weight gelator hydroxystearic acid (HSA) is added; this formulation enables the preparation of a photonic crystal in the physical gel state (*37*).

Photo-polymerizable LC formers or "reactive mesogens" (*38*, *39*) are frequently used in BP formulations. Reactive mesogens are part of the materials shown in Fig. 3 (C and D). Figure 3C shows a BP formulation consisting of reactive mesogen RM82, cyanobiphenyl nematic mixture HTG135200, chiral dopant R5011, cross-linker TMPTA, and photo-initiator I-651 (*14*). The formulation can be photopolymerized to form a chemical gel. In the photopolymerized gel, all components other than the cyanobiphenyl species are polymerized. The physical gel in Fig. 3B can reversibly transition between different phases (e.g. BP ⇌ Iso), while the cross-linked polymer formed from the materials shown in Fig. 3C does not exhibit phase transitions; photopolymerization of the Fig. 3C formulation "freezes" the BP structure.

Fully solid BPs have recently been realized. When the mixture in Fig. 3D is photopolymerized and the nonreacting components are subsequently washed out, a fully solid, elastomeric BP is formed (*40*). The elastomeric nature of the BP arises from using a dithiol, which cross-links the mixture lightly. The elastomer can be strained 150% and exhibits color change upon extension. BPs can also be dispersed as liquid droplets in polymeric matrices (*41*, *42*). Dispersed LC droplets are interesting for sensing applications, as they produce detectable optical changes at much lower analyte concentrations than LC films (*8*). BP droplets in an aqueous medium have also been prepared (*43*) and are compelling responsive materials (*6*).

In summary, BPs can be used to form soft photonic crystals in a variety of physical states, which have vastly different mechanical properties. The rich diversity of BP formulations gives access to a broad spectrum of soft photonic crystals that vary in their mechanical properties.

STIMULI-RESPONSIVE PHOTONIC CRYSTALS

BPs combine photonic crystallinity with stimuli responsiveness and are therefore compelling materials for a broad range of applications. We discuss below the properties and applications of BP-based photonic polymers.

Mechanical deformation alters the dimensions of polymerized BP lattices, causing changes in color (*40*, *44*). The response of BP gels and elastomers to strain is shown in Fig. 4. In Fig. 4A, a BP gel is strained in a tensile geometry. Tensile uniaxial deformation causes reduction of the lattice size in the viewing direction, resulting in the observed blue shift (*44*). The gel shown in Fig. 4A can be strained 50%. BP elastomers, prepared by White and coworkers, in contrast, can be strained to nearly 150%. The deformation of both BP gels and elastomers has been reported to be reversible (*40*, *44*); the critical strain for reversibility, however, has not been determined.

BP elastomers are interesting model systems for deformation studies owing to the large strain that can be accommodated in these systems (*40*). The mechanical deformation of a BPII elastomer with (100) lattice orientation is shown in Fig. 4B. Photographic images and UV-visible transmission spectra are shown for the elastomer at incidence angles of 0° and 45°. The dashed and solid lines represent spectra collected at normal and 45° incidence, respectively. The peak in the dashed curves corresponds to the (100) reflection; as expected, this reflection exhibits a blue shift upon strain. Reflection from either the (010) or (001) lattice plane is observed at 45°; this reflection red shifts upon strain, resulting in the green color observed visually. Performing measurements at multiple incidence angles captures the asymmetric nature of lattice deformation in strained BPs. White and coworkers also strain the elastomers biaxially. The structures generated through biaxial tensile deformation of BP polymers remain to be understood. No studies exist, to the best of our knowledge, which investigate the change in BP

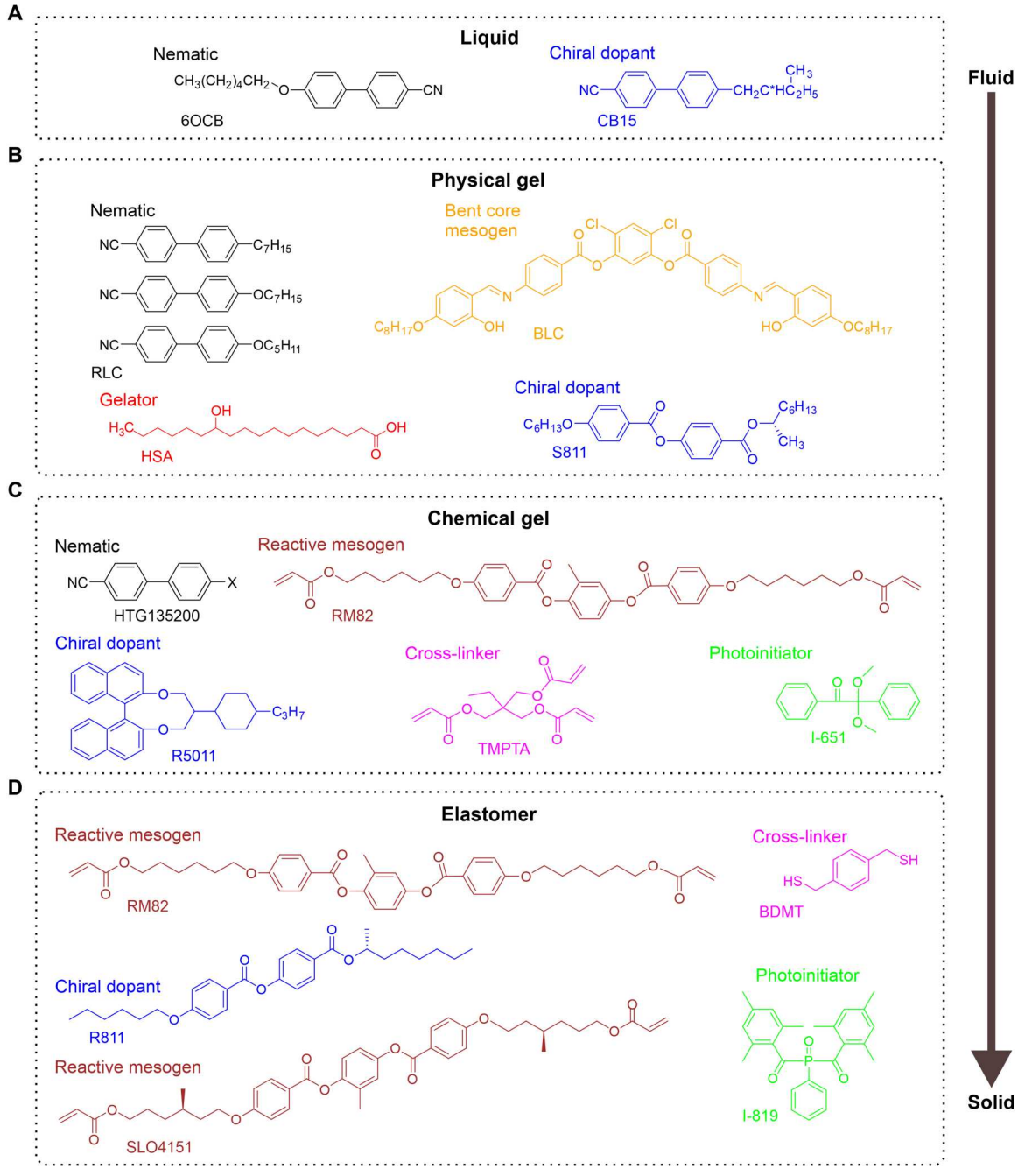

Fig. 3. Chemical composition of BP-forming systems. BP formulations that can form (**A**) liquid (*36*), (**B**) physical gel (*37*), (**C**) chemical gel (*14*), and (**D**) elastomeric photonic crystals (*40*). Molecules are colored based on function; nematic LC formers are colored black, chiral dopants are colored blue, photo-initiators are colored green, cross-linkers are colored pink, reactive mesogens (photopolymerizable mesogens) are colored brown, the low–molecular weight gelator is colored red, and the bent-core mesogen is colored orange.

structure upon compression. There are therefore several research opportunities in understanding the structures generated through mechanical deformation of BPs.

BPs respond to electric fields by changing color. Polymerized BPI monocrystals have been demonstrated to exhibit a red shift in response to an electric field applied perpendicular to the sample (*45*), as shown in Fig. 4C. Lattice expansion occurs along the direction of the applied electric field. Lattice expansion can be observed both visually and in the reflection spectrum as shown in Fig. 4C. Electric fields can also be used to erase the photonic bandgap of BPs, as shown in Fig. 4D, where an electric field is used to reversibly switch the color of a BPII chemical gel from green to colorless (*46*). The strong electric field introduces homeotropic anchoring in the nonpolymerized fraction of the gel, thereby destroying the BP structure. On removal of the field, the system reverts to its original

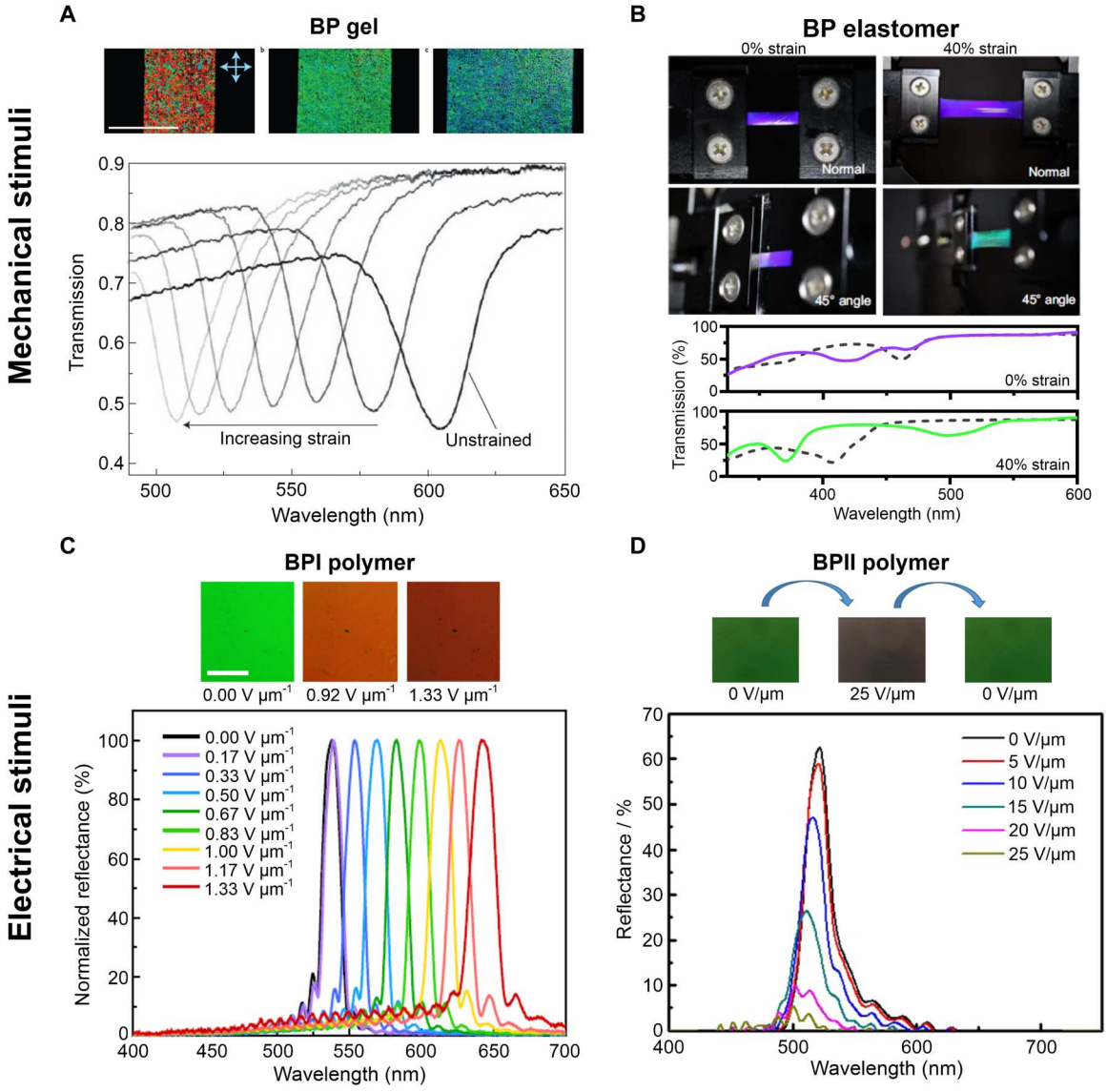

Fig. 4. Stimuli-responsive, polymerized BPs. Polymerized BPs respond to mechanical (**A** and **B**) and electrical stimuli (**C** and **D**) by changing color. (A) POM images and reflection spectroscopy of as-prepared and strained BP gel. Reproduced with permission from (*44*). Copyright 2014 Nature Publishing Group. (B) Photographic images and reflection spectroscopy of as-prepared and strained BP elastomer. The dashed and solid lines represent spectra collected at normal and 45° incidence, respectively. Reproduced with permission from (*40*). Copyright 2021 Nature Publishing Group. (C) Optical images and reflection spectroscopy of BP polymer I at different electric fields. Reproduced with permission from (*45*). Copyright 2017 Nature Publishing Group. (D) Optical images and reflection spectroscopy of BP polymer II at different applied electric fields. Reproduced with permission from (*46*). Copyright 2017 American Chemical Society.

structure. Both the BPI and BPII samples shown in Fig. 4 (C and D) are chemical gels.

The response of polymerized BPs to electric fields depends on material properties such as dielectric anisotropy (Δε) and gel fraction (polymerized fraction). A careful selection of materials is required to engineer the desired response of BPs to electric fields. A large magnitude of dielectric anisotropy results in response to electric fields at lower voltages (*19*), while the sign determines whether the molecular long axis orients along (Δε > 0) or perpendicular (Δε < 0) to the applied field. The response shown in Fig. 4D is characteristic of a material with positive dielectric anisotropy (*46*). The fraction of polymerized material also needs to be carefully optimized for a desirable set of material properties. While polymerization improves the thermal stability and mechanical robustness of BPs, it hinders fast response to stimuli. BPs, where the polymerized species is about 10 weight % or less, have been shown to exhibit submillisecond response times while exhibiting far greater thermal stability than their liquid counterparts (*46*, *47*).

Materials that change color in response to chemical stimuli form the basis of colorimetric sensors. The response of polymerized BPs to chemical stimuli is intimately linked to the composition of the BP-forming material. A humidity-sensitive BP-based chemical gel is shown in Fig. 5A (*21*). The authors use carboxylic acid–based reactive mesogens in their formulation (see 4OBA and 6OBA in

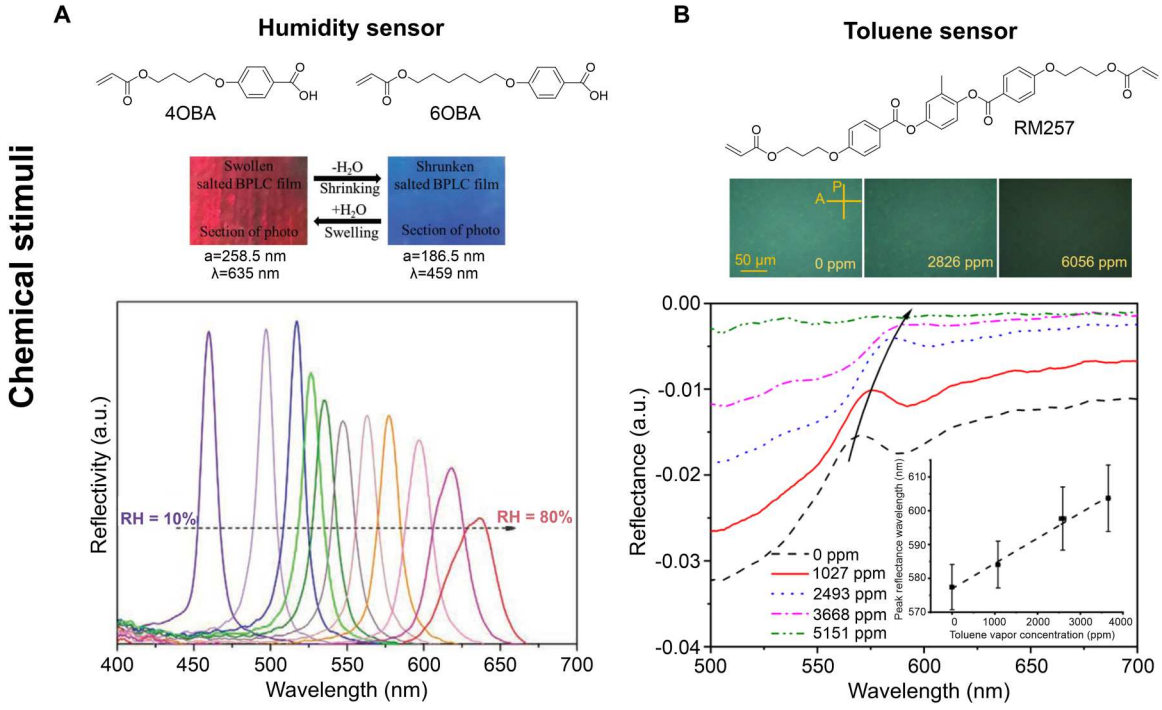

Fig. 5. Colorimetric sensors based on polymerized BPs. (**A**) Optical image and reflection spectroscopy of a BP polymer at different relative humidity. The carboxylic acid–based reactive mesogens depicted in the figure are converted to potassium salts, making the material humidity sensitive. Reproduced with permission from (*21*). Copyright 2020 WILEY-VCH Verlag GmbH & Co. KGaA, Weinheim. (**B**) POM images and reflection spectroscopy of a BP polymer at different toluene vapor concentrations. The molecular structure of RM257, the reactive mesogen used in the toluene-sensitive formulation, is depicted above the POM images. Reproduced with permission from (*22*). Copyright 2020 American Chemical Society.

Fig. 5A). The carboxylic acid is transformed to a potassium salt by immersion in an aqueous potassium hydroxide solution; after the conversion process, the film is dried. The resulting material is hydrophilic. Absorption of water results in lattice expansion and a red shift in the photonic bandgap. The reflection spectrum as a function of relative humidity is shown in Fig. 5A. A polymerized BP that expands in toluene vapor is shown in Fig. 5B. The BP-based colorimetric sensor, prepared by Abbott and coworkers (*22*), can detect toluene concentrations as low as 140 ppm. For toluene, OSHA (The Occupational Safety and Health Administration) recommends human exposure levels less than 200 pm over an 8-hour period; the BP-based sensor shown in Fig. 5B would be sensitive to exposure at these levels. Chemical swelling of polymerized BPs has been observed for other organic compounds as well, such as acetone (*40*). As BPs are composed of organic materials, they usually interact with and respond to organic analytes.

In summary, the polymeric derivatives of BPs can be responsive to mechanical, chemical, and electrical stimuli. Response to all these stimuli produces changes in color. The tendency to produce color changes in response to stimuli can be exploited for a broad range of applications such as sensing (*22*), artificial camouflage (*48*), and display technology (*49*).

CONTROL OF LATTICE ORIENTATION IN BPs

Establishing approaches to form single crystals has been one of the central focuses of the BP research field. The interest in single-crystalline BPs arises from their superior material properties. Unlike their polycrystalline counterparts, single-crystalline BPs exhibit spatially uniform optical properties. The use of lattice-aligned BPs in devices also results in lowered operating voltages and reduced hysteresis (*17*).

We describe four approaches that have been used successfully to assemble BPs with a high degree of lattice alignment, namely, (i) the gradient temperature technique (*45*), (ii) the application of electric fields (*37*), (iii) the use of photoalignment layers (*50*), and (iv) the use of chemical patterns (*51*). After a brief description of each of these techniques, we compare the different approaches of growing single-crystalline BPs. Although rubbed polyimide (*52*) has been used to align BPs, we do not discuss it here; rubbed polyimide and photoalignment both provide directional planar anchoring, obviating the need to discuss them separately.

The gradient temperature scanning (GTS) technique has been used to grow BPI single crystals with lateral dimensions on the order of a centimeter. Figure 6A shows the gradient temperature stage used by Lin and coworkers (*45*). The stage consists of two blocks and a gap between them. One of the blocks is held at a slightly higher temperature, creating a thermal gradient. The sample, which consists of mesogens sandwiched between rubbed polyimide glass slides, is pulled from the high to low temperature region. Creating the thermal gradient allows for BPI monocrystals to grow from BPII polycrystals. Using the gradient temperature stage, the authors observe formation of a 0.1-mm-thick BPI single crystal formed over an area of ~10 × 5 mm^2. The GTS technique is analogous to the Czochralski method (*53*–*55*) used to grow large single crystals of inorganic semiconductors. Although large monocrystals can be

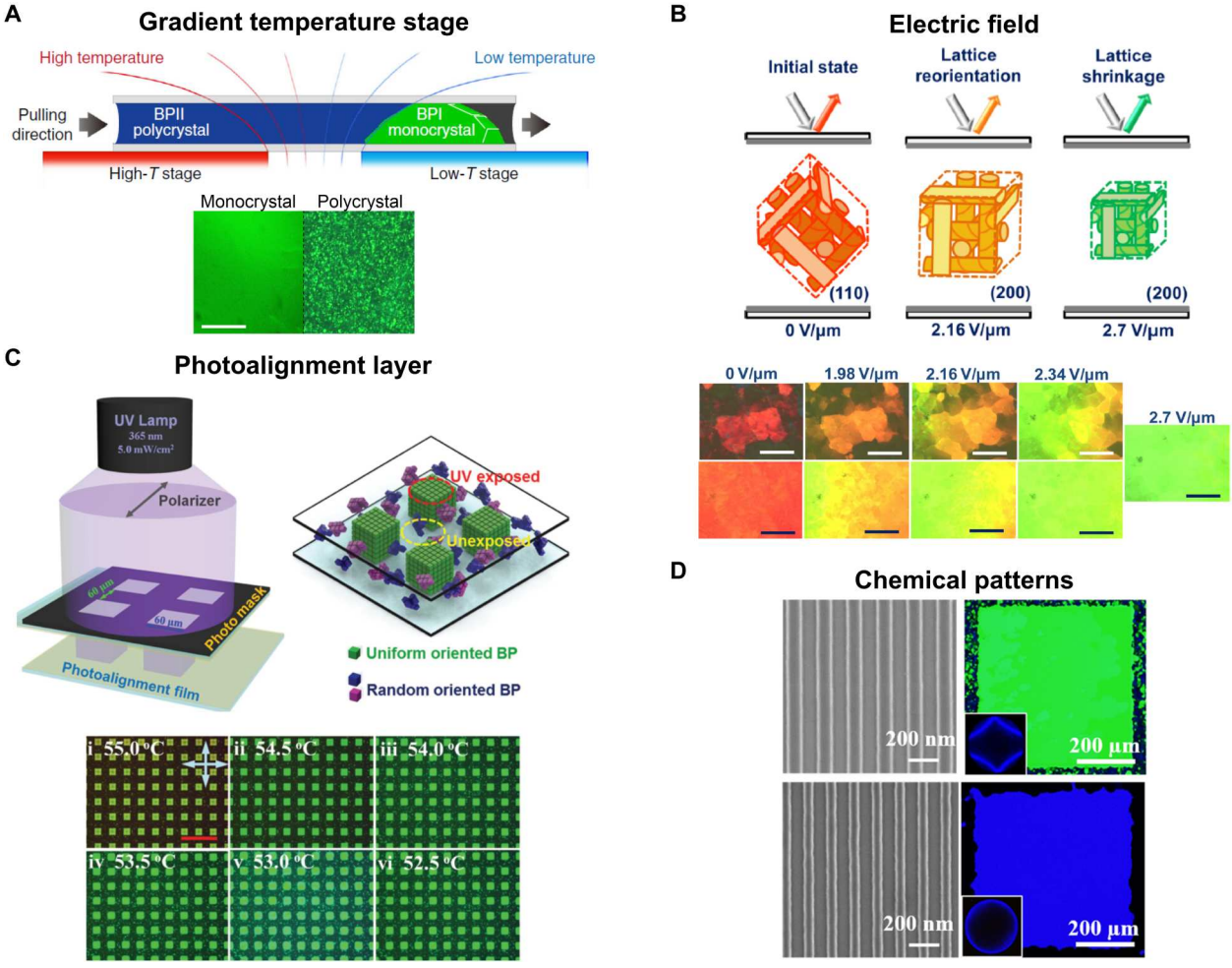

Fig. 6. Different strategies to control lattice orientation in BP LCs. Controlling lattice orientation using (**A**) the gradient temperature technique; a BPI single crystal grows from the polycrystalline precursor BPII phase (**B**) electric fields; the torque from the electric field reorients the (110) oriented domains to (200) (**C**) photoalignment layers; directional planar alignment is obtained by exposing a photosensitive layer to linearly polarized light and (**D**) chemical patterns; alternating homeotropic and planar regions assemble single crystals by reducing elastic distortions for a targeted lattice orientation. Panel (A) is reproduced with permission from (*45*). Copyright 2017 Nature Publishing Group. Panel (B) is reproduced with permission from (*37*). Copyright 2017 American Chemical Society. Panel (C) is reproduced with permission from (*50*). Copyright 2017 WILEY-VCH Verlag GmbH & Co. KGaA, Weinheim. Panel (D) is reproduced with permission from (*58*). Copyright 2019 American Chemical Society.

obtained from the GTS technique, it is restricted to BPI and has hitherto provided access to only one single-crystal lattice orientation.

Electric fields have been used to control lattice orientation in BPs (*37*). Figure 6B shows an example where an electric field of ~3 V/μm was used to obtain uniform (200) orientation of a BPI physical gel. In this case, the electric field induces reorientation of domains from (110) to (200). The study used the mixture shown in Fig. 3B. Vertical field switching cells, using electric fields of ~2 V/μm, have also been used to align BPs (*56*).

Photoalignment layers based on azobenzenes have been used to control the lattice orientation of BPs. Photoalignment involves exposing a thin layer of azobenzene-based small molecule or polymer adhered to the substrate to linearly polarized light. The BP-forming material is introduced after photo-treatment of the alignment layer. Both the White (*40*) and Li (*50*) groups have used photoalignment layers to assemble BPII with (100) orientation. BPII crystals with (100) lattice orientation that were prepared on photoalignment layers are shown in Fig. 6C. The mechanism of BP alignment on photoalignment layers, which provide planar anchoring, is unclear.

Chemical patterns consisting of alternating homeotropic and planar anchoring regions have been used to assemble single crystals of both BPI and BPII (*51*, *57*, *58*). BP single crystals assembled from chemical patterns are shown in Fig. 6D. A given chemical pattern minimizes elastic distortions for the targeted lattice orientation. The theoretical basis for the design of the chemical patterns is discussed in detail in the next section. Figure 6D shows green BPI and blue BPII single crystals formed on patterns consisting of alternating homeotropic and planar regions. The chemical patterns consist of alternating regions of silicon and a side-chain liquid crystalline brush, PMMAZO [poly(6-(4-methoxy-azobenzene-4′-oxy) hexyl methacrylate)]. Silicon anchors mesogens in a planar manner, while PMMAZO, at the used grafting density, provides homeotropic anchoring (*59*, *60*). Figure 6D shows scanning electron microscopy (SEM) images of the chemical patterns used to assemble the BPs. While the patterns shown in the figure are formed using electron

beam lithography, their dimensions are large enough that they can be easily prepared through large-area patterning techniques such as interference lithography (*61*, *62*).

Directed self-assembly of BPs on chemical patterns offers access to a larger number of single-crystal lattice orientations than any other method. In the BPII regime, single crystals with (100), (110), and (111) lattice orientation can be obtained by changing the pattern geometry (*51*). Moreover, single crystals of both BPI and BPII can be assembled on chemical patterns as shown in Fig. 6D. While BP assembly on chemical patterns offers the largest range of single-crystal structures, the gradient temperature method has been used to grow the largest single-crystal samples, in terms of both thickness and area. While the thickest single crystals assembled using chemical patterns are ~30 μm (*63*), 100-μm-thick $BPI_{(110)}$ monocrystals have been grown using the gradient temperature technique (*45*).

One of the chief advantages of preparing functional materials from BPs is the large area and thickness over which single crystals can be formed. For other self-assembling soft materials such as block copolymers (BCPs), the timescale of organization into ordered states grows drastically with film thickness (*64*, *65*); for micrometer-scale BCP films, ordered states require annealing for days and are therefore kinetically inaccessible. For BP LCs, single-crystalline assemblies that are approximately ~30 μm thick can be prepared in a couple of hours (*63*) owing to the fast dynamics in the liquid state. Conversion of lattice-aligned BP LCs into polymeric states enables large-volume fabrication of homogeneous, mechanically robust, and responsive photonic materials. The properties of new soft materials derived from BPs, discussed in the final section, would also be enhanced by the macroscopic dimensions over which BP single crystals can be assembled.

COMPUTER SIMULATIONS OF BPs

Continuum simulations make powerful predictions about the thermodynamics of BP self-assembly. Simulations can therefore be used to guide experimental design and discovery of BP-based materials. For instance, simulations have played an important role in identifying strategies to control the lattice orientation of BPs, which was discussed in depth in the earlier section.

In this section, we review the theoretical basis of continuum, LdG-based simulations of BP LCs. We then go on to highlight two examples where simulations were used to accurately predict experimentally observed behavior, namely, (i) the assembly of BP single crystals on nanopatterned substrates and (ii) the segregation of nanoparticles to specific locations in the defect network of the BPII lattice. These examples highlight the power of using continuum simulations for computational design of BP-based functional materials.

The Q tensor formalism can be used to describe the thermodynamics of BP LCs. The Q tensor, which describes the ordering of an LC state, is given by the expression

$$Q_{ij} = S\left(n_i n_j - \frac{1}{3}\delta_{ij}\right) \tag{3}$$

where δ_{ij} is the Kronecker delta, n_i with $i = x,y,z$ represents a component of the local director, $\boldsymbol{n}$, and S is the scalar order parameter and is given by the equation

$$S = \frac{1}{2}\langle 3\cos^2(\theta) - 1\rangle \tag{4}$$

with $\cos\theta = \boldsymbol{a}\cdot\mathbf{n}$, where $\boldsymbol{a}$ is the molecular orientation given by the main molecular axis, and $\langle\ \rangle$ denotes a spatial average.

Short-ranged (f_p), elastic (f_e), and surface interactions (f_s) all contribute to the free energy of BPs. The total free energy density is given by the equation

$$F(\boldsymbol{Q}) = \int \mathrm{d}^3x[f_P(\boldsymbol{Q}) + f_E(\boldsymbol{Q})] + \int \mathrm{d}^2x f_S(\boldsymbol{Q}) \tag{5}$$

On the basis of LdG theory, the following expression is proposed to account for short-range interactions

$$f_P = \frac{A}{2}\left(1 - \frac{U}{3}\right)\mathrm{tr}(\boldsymbol{Q}^2) - \frac{AU}{3}\mathrm{tr}(\boldsymbol{Q}^3) + \frac{AU}{4}\mathrm{tr}(\boldsymbol{Q}^2)^2 \tag{6}$$

where A and U are phenomenological quantities.

The elastic contribution to the free energy is given by the expression

$$f_E = \frac{1}{2}\left[L\frac{\partial Q_{ij}}{\partial x_k}\frac{\partial Q_{ij}}{\partial x_k} + 2Lq_0\epsilon_{ikl}Q_{ij}\frac{\partial Q_{lj}}{\partial x_k}\right] \tag{7}$$

where $q_0 = 2\pi/p$ is the inverse pitch, L is the elastic constant, and ϵ_{ikl} is the Levi-Civitia tensor. The expression for elastic free energy shown in Eq. 7 arises from making the one-elastic constant assumption. While the first term in Eq. 7 is common to both chiral and nonchiral LC phases, the second term vanishes for nonchiral systems.

The surface contributions to free energy (*66*, *67*) are given by the following equations, based on whether the anchoring is planar (P) or homeotropic (H)

$$f_S^P = W_P(\tilde{\boldsymbol{Q}} - \tilde{\boldsymbol{Q}}^{\perp})^2 \tag{8}$$

$$f_S^H = 1/2W_H(\boldsymbol{Q} - \boldsymbol{Q}^0)^2 \tag{9}$$

where W_P and W_H are the anchoring energies for planar and homeotropic surfaces, respectively. In Eq. 8, $\tilde{\boldsymbol{Q}} = \boldsymbol{Q} + \frac{1}{3}S\boldsymbol{I}$ and $\tilde{\boldsymbol{Q}}^{\perp} = \boldsymbol{P}\tilde{\boldsymbol{Q}}\boldsymbol{P}$, where $\boldsymbol{I}$ is the identity matrix and $\boldsymbol{P}$ is the projection operator given by $P_{ij} = \delta_{ij} - \nu_i\nu_j$ and where $\boldsymbol{\nu}$ is the vector normal to the surface. In Eq. 9, $\boldsymbol{Q}^0$ represents the surface-preferred tensor order parameter. The minimization of free energy can be accomplished using the Landau-Ginzburg method wherein $\boldsymbol{Q}$ evolves toward equilibrium according to (*66*)

$$\frac{\partial \boldsymbol{Q}}{\partial t} = -\frac{1}{\gamma}\left[\boldsymbol{\Pi}\left(\frac{\delta F}{\delta \boldsymbol{Q}}\right)\right] \tag{10}$$

where γ is the rotational viscosity. Here, the operator $\boldsymbol{\Pi}$ acting on a given matrix $\boldsymbol{M}$ is given by $\Pi(\boldsymbol{M}) = \frac{1}{2}(\boldsymbol{M} + \boldsymbol{M}^T) - \frac{1}{3}\mathrm{tr}(\boldsymbol{M})\boldsymbol{I}$. The operator $\boldsymbol{\Pi}$ ensures the symmetric and traceless properties of the $\mathbf{Q}$ tensor. The boundary conditions are given by $\boldsymbol{\Pi}\left[\left(\frac{\delta F}{\delta \nabla \boldsymbol{Q}}\right)\cdot\boldsymbol{\nu}\right]$. The minimization procedure can be performed using either the finite difference or the finite element method. For BPs, it is convenient to start from an ansatz. Thus, initial conditions (*68*, *69*) for

BPI are given by

$$Q_{xx} = A\ [-\sin(ky/\sqrt{2})\ \cos(kx/\sqrt{2}) - \sin(kx/\sqrt{2})\ \cos(kz/\sqrt{2}) + 2\sin(kz/\sqrt{2})\cos(ky/\sqrt{2})] \quad (11a)$$

$$Q_{xy} = A\ [-\sqrt{2}\sin(kx/\sqrt{2})\ \sin(kz/\sqrt{2}) - \sqrt{2}\cos(ky/\sqrt{2})\ \cos(kz/\sqrt{2}) + \sin(kx/\sqrt{2})\cos(ky/\sqrt{2})] \quad (11b)$$

while for BPII

$$Q_{xx} = A\ (\cos kz - \cos ky) \quad (12a)$$

$$Q_{xy} = A\ \sin kz \quad (12b)$$

where A represents the amplitude of initialization, $k = 2q_0r$ corresponds to the strength of the chirality where r is the red shift, which was found to be 0.71 for BPI and 0.86 for BPII. In all cases, the components yy, zz, xz, and yz are obtained by cyclic permutation of those given above. The BP lattice parameters, a_{BPI} and a_{BPII}, depend on the chiral pitch and the appropriate red shift via $a_{BPI} = \frac{p}{\sqrt{2}r}$, $a_{BPI} = \frac{p}{2r}$. The principles of continuum, free energy–based simulation of BPs are summarized in Fig. 7.

Computer simulations have been used to design surfaces that promote the growth of BP single crystals (*51*). When BPII with (100) orientation is placed on a homeotropic surface, alternating ordered and disordered regions are visible in the computationally calculated order parameter map, as shown in the inset of Fig. 8A. For the (111) lattice orientation of BPII, a hexagonal order parameter pattern is visible, as shown in the inset of Fig. 8C. Continuum simulations predict that when a chemical pattern resembles the order parameter map for a given lattice orientation, that orientation is thermodynamically favored; a chemical pattern that mirrors the order parameter map relieves elastic distortions. Figure 8 shows SEM images of chemical patterns designed to resemble the computationally calculated order parameter maps for the (100), (110), and (111) lattice orientations of BPII. The POM images in Fig. 8 show that these patterns successfully assemble BP single crystals with different targeted lattice orientation. The pattern periodicity also plays an important role in the assembly of BP single crystals. Continuum simulations predict and experiments on a broad range of BP-forming materials (*70*) verify that when the striped pattern periodicity equals the unit cell size of BPII, a single crystal with (100) orientation forms (Fig. 8A).

Continuum simulations make predictions about the structure of nanoparticle-doped BPs (*71*). The variation of the free energy density within the BPII unit cell is shown in Fig. 9A (*71*). The free energy is the highest at the intersection point of the disclinations, and this region, therefore, is expected to have the maximum propensity to attract nanoparticles. The free energy is also higher at all points along the disclination network than in the DTC region. X-ray scattering studies by Reven and coworkers (*36*) reveal that when functionalized gold nanoparticles are doped into BPII, they segregate to (i) the intersection point of the disclinations and (ii) the midpoint of the disclination arms (the ends being defined as the meeting points of the tetrahedral arms of the disclination network). The x-ray scattering pattern from the BPII-nanoparticle composite and the corresponding structure are shown in Fig. 9, B and C, respectively. The x-ray scattering pattern can be explained by a combination of two nanoparticle lattice structures: a BCC lattice structure where the nanoparticles only occupy the

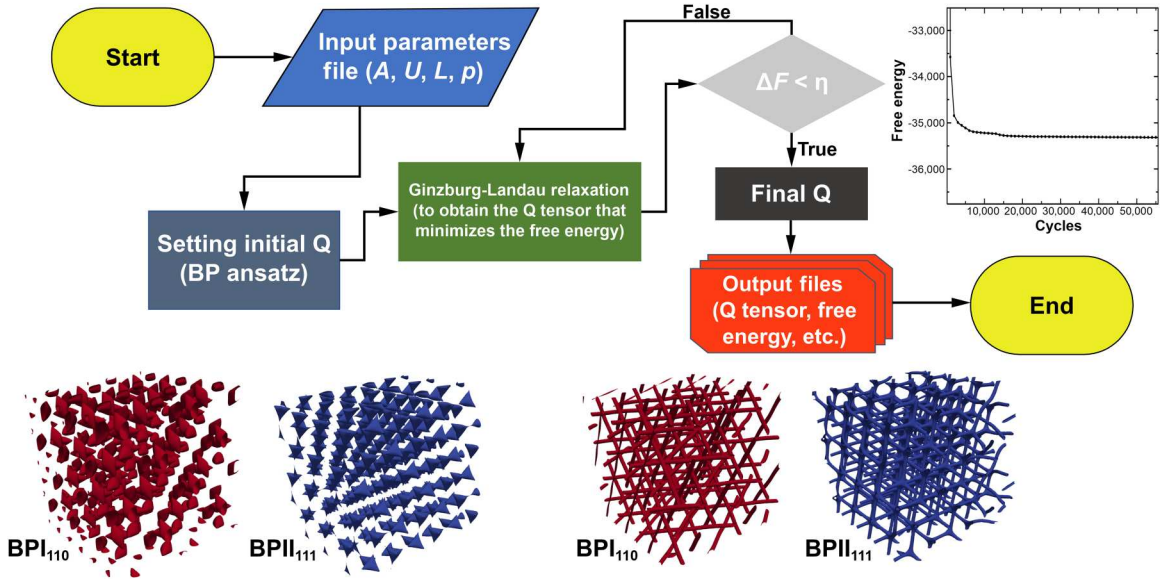

Fig. 7. Flowchart for continuum, LdG-based simulations. Prerequisites for the simulation include input parameters such as system size, confinement geometry, anchoring conditions, and material properties such as pitch (p), elastic constant (L), and phenomenological constants A and U that come from LdG theory. Given the initial conditions, the purpose of the simulation is to find the Q tensor that minimizes the free energy, F. Identification of the minimum energy state is accomplished by the Ginzburg-Landau relaxation procedure. We assume that the system has reached a minimum free energy state when the free energy difference, ΔF, between one simulation cycle and the previous is less than a sufficiently small number η (typically ~10^{-9}).

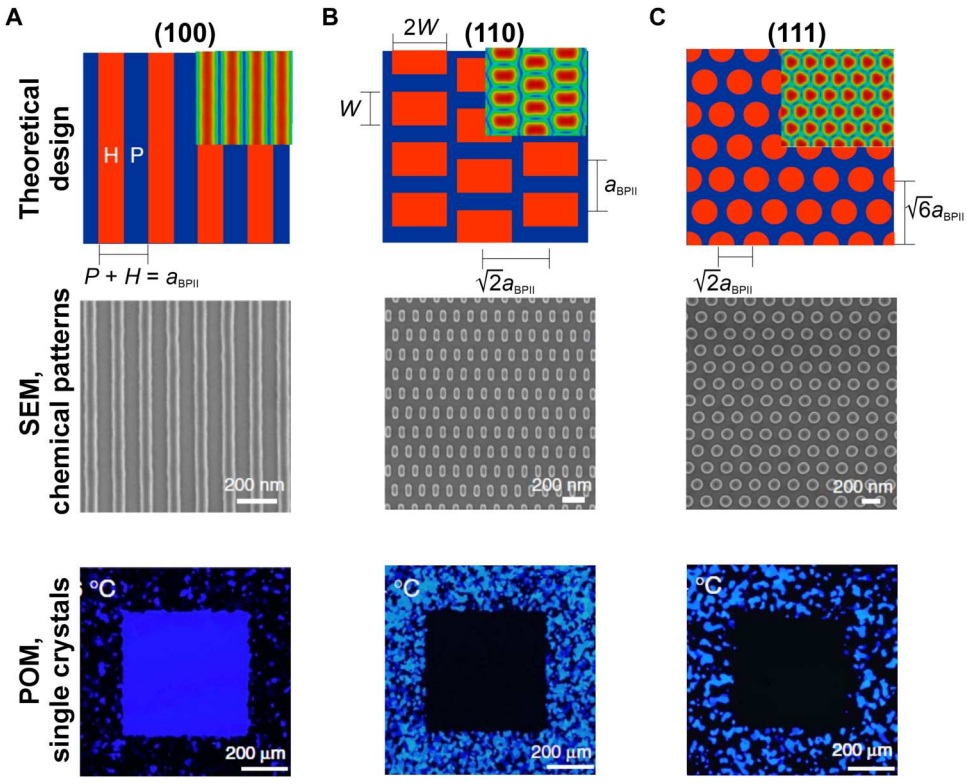

Fig. 8. Directed self-assembly of BPII on chemical patterns. Pattern designs (top), SEM images of chemical patterns (middle), and POM images (bottom) for (**A**) (100), (**B**) (110), and (**C**) (111) single crystals. H and P represent homeotropic and planar surfaces, respectively. a_{BPII} represents the lattice size of BPII. Chemical patterns are designed to mirror the order parameter maps for a given lattice orientation; the order parameter maps are shown in the inset of the images in the top row. Stripe, rectangular, and circular chemical patterns lead to the formation of (100), (110), and (111) single crystals, respectively. Chemical pattern designs that are based on continuum simulations successfully grow single crystals with targeted lattice orientation. Reproduced with permission from (*51*). Copyright 2017 Nature Publishing Group.

intersection points of the tetrahedral disclination arms and a four-particle lattice configuration (4PC), where nanoparticles occupy the midpoint of the disclination lines. Both lattices were theoretically predicted as possible nanoparticle structures in BPs (*71*).

Simulations predict that the lattice structure of nanoparticles in BPs is dependent on particle size (*71*). Nanoparticles smaller than 100 nm are predicted to assemble into a face-centered cubic lattice in BPI. For particles larger than 100 nm, a BCC colloidal lattice is predicted. Simulations also make predictions about the influence of anchoring energy of the nanoparticle surface on the structure of the composites. Experimental verification of these predictions could be a fruitful direction for researchers working on BPs.

Numerical simulations can be used to predict the response of BPs to external driving forces, such as pressure gradients and electric fields. Hydrodynamics has been incorporated into the LdG formalism, enabling prediction of BP structures formed in response to flow. Henrich and coworkers (*72*) have made predictions about the structure of BPs in microfluidic channels; experimental testing of these theoretical predictions could be an interesting area of future investigation. Electric fields can also be accounted for in an LdG-based free energy description of BPs (*73*). Simulations can therefore be used to guide experimental efforts in using electric fields to manipulate BP structure.

Simulations of BPs have hitherto relied on a continuum-level description. Although continuum simulations are highly successful in predicting the macroscopic behavior of BPs, they lack molecular details. The rapid advances in computational power have enabled molecular dynamics simulations of systems with ~50 million atoms (*74*). It is therefore conceivable that both coarse-grained and atomistic simulations of BPs shall be realized soon. Molecular simulations could enable a deeper understanding of the structure of BPs. As discussed in earlier sections, most BP formulations are complex multicomponent mixtures. Molecular simulations could be used to characterize compositional heterogeneity in the BP unit cell. Further, molecular dynamics simulations could be used to quantify dynamic heterogeneity in BPs. As disclinations have a different structure from DTCs, it is reasonable to expect different molecular relaxation times in these regions.

BP-BASED NANOCOMPOSITES

In the last section, we discussed the use of simulations to make powerful predictions about the self-assembly of nanoparticles in BPs. We discuss below BP-based nanocomposites from an experimental perspective.

Disclinations template nanoparticle self-assembly in BPs. An example of the highly structured nanoparticle lattices that can form in BPs is shown in Fig. 9. As discussed earlier, dopants in a BP matrix tend to segregate to disclinations owing to their higher local free energy (Fig. 9A). By occupying these high energy regions, nanoparticles enhance the thermal stability of BPs. A variety of nanoscale additives such as carbonaceous nanoparticles

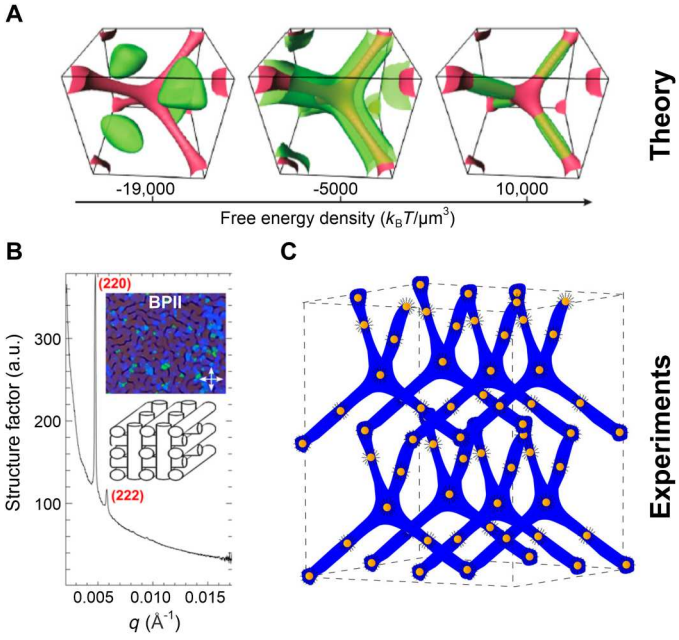

Fig. 9. Directed self-assembly of nanoparticles in BPs. (**A**) The free energy density variation within the BPII unit cell. The red and green areas represent high and low free energy regions, respectively. Reproduced with permission from (*71*). Copyright 2011 National Academy of Sciences. (**B**) X-ray scattering profile of gold nanoparticles doped in BPII. (**C**) Schematic representation of the structure of BP nanoparticle composite inferred from x-ray scattering. Continuum simulations can be used to predict the binding sites of nanoparticles in BPs. Panels (B) and (C) are reproduced with permission from (*36*). Copyright 2016 American Chemical Society.

(*75*) (C60, carbon nanotubes, and graphene oxide), magnetic nanoparticles (*76*), ferroelectric nanoparticles (*77*), and quantum dots (*78*) have been incorporated into BPs. For all these different systems, the addition of nanoparticles at an optimal concentration broadens the temperature range over which BPs are stable. The introduction of nanoparticles has been shown to reduce hysteresis (*77*) and lower operating voltages (*78*) in BP-based LCD devices.

The nanoparticle lattice has a different symmetry compared to the BP medium in both BPI and BPII (*36*). The presence of two different lattice symmetries in the same material could be exploited to prepare tunable photonic crystals (*79*). Moreover, as the arrangement of the disclinations is different in BPI and BPII, the nanoparticle lattices that form in these phases are different. Thermally cycling between BPI and BPII can result in switching between different nanoparticle lattices. Facile reconfigurability is an advantageous feature of nanoparticle lattices created in BP matrices.

The incorporation of nanoparticles into polymerizable BPs can be used to create technologically and fundamentally interesting materials. Recently, Yadav *et al.* (*80*) have shown that the addition of CdTe quantum dots to polymerized BPs increases the transmittance, dielectric permittivity, and Kerr constant (relative to the undoped polymer). All these parameters are vital to LCD device performance. Immobilizing nanoparticle assemblies in BPs through photopolymerization also presents opportunities for creating highly structured polymer nanocomposites. Achieving controlled dispersion of nanoparticles is an area of intense research in the field of polymer nanocomposites (*81*, *82*); BP-derived materials could be of interest to researchers in this field. While researchers have created BP-based polymer nanocomposites (*80*, *83*), the organization of nanoparticles within the polymer has not been fully elucidated using structural techniques such as x-ray scattering and electron microscopy. For liquid BPs, it is agreed that nanoparticles occupy the disclination regions. The influence of polymerization on nanoparticle organization has, however, remained largely unexplored. Moreover, while the optical properties of BP-based nanocomposites have been investigated, the impact of nanoparticle addition on the mechanical properties has remained unstudied.

FUTURE DIRECTIONS

We discuss below potential research opportunities involving BPs. Specifically, we discuss the possibilities of using the BP structure as a template to prepare (i) polymer meshes and (ii) inorganic

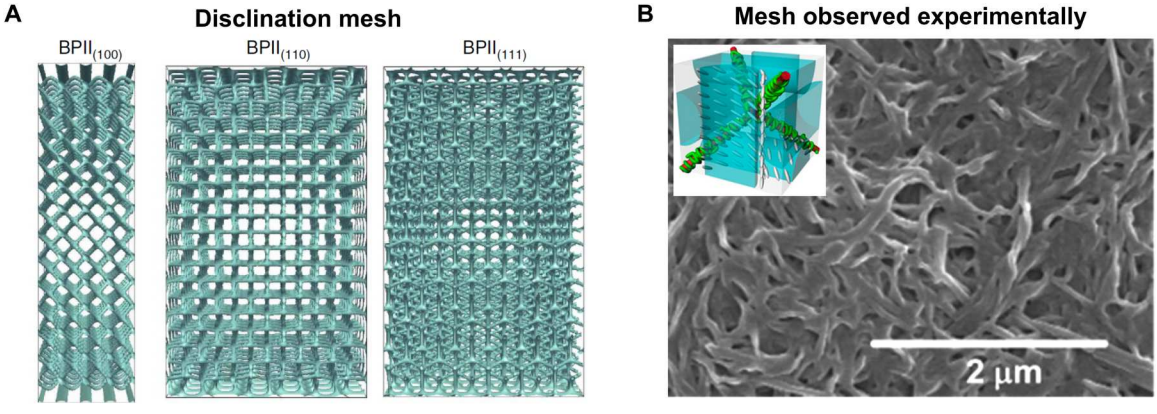

Fig. 10. Disclination templated polymerization of BPs. (**A**) The disclination network of BPII for (100), (110), and (111) lattice orientations. Reproduced with permission from (*51*). Copyright 2017 Nature Publishing Group. (**B**) SEM image of a polymeric mesh prepared from a BP LC. Reproduced with permission from (*46*). Copyright 2017 American Chemical Society. A BPII gel is washed out to generate the mesh structure seen in the image. The inset shows the proposed mechanism of polymerization. In principle, polymeric meshes that look like the disclination networks could be prepared. In practice, the experimental structures are far more disordered than the disclination mesh in the unpolymerized BP liquid.

photonic crystals. We also discuss opportunities in discovery of (iii) new BP symmetries and in understanding (iv) compositional heterogeneity in BPs.

Highly structured polymer meshes from BP templates

BPs have a regular organization of disclination defects. As shown in Fig. 10B, the disclinations in BPII form a network structure. Selective polymerization of disclinations in BPII and subsequent removal of the unpolymerized DTC regions can, in principle, be used to synthesize highly regular polymeric meshes. The development of bottom-up strategies for creating polymers with monodisperse and structured pores is an active area of research. Both LCs (*84*) and BCPs (*85*) have been used to prepare porous polymers with highly controlled pore size and structure. However, the symmetry of the porous structure that could be achieved from using BPII cannot be attained by using BCPs or any other liquid crystalline phase. We summarize below the past mechanistic work on polymerization of BPs as well as challenges in obtaining regular pore structures.

Disclinations template polymerization in BP LCs. X-ray scattering studies have shown that the polymerized fraction of a BP gel has the same symmetry as the disclination network (*86*). Imaging studies reinforce the picture derived from scattering measurements. A SEM image of a polymerized BP, where the nonpolymerized portions are washed out in a solvent, is shown in Fig. 10B (*46*). In BPII, the disclinations form a network. The polymerized BP also exhibits a network structure, supporting the picture that polymerization in BP is templated by the disclination network.

The polymeric meshes prepared from BPII are quite irregular compared to the highly structured network of disclinations, shown in Fig. 10A. The disorder in polymeric meshes could arise from (i) polycrystallinity, (ii) collapse of network structure during washing out unpolymerized portions, and (iii) cross-linking the disclination network. While several strategies exist to create BP single crystals, as discussed earlier, the challenge in creating structures like those shown in Fig. 10A lies in retaining mechanical integrity after washing out the unpolymerized regions. Optimizing the nature and fraction of the polymerizable species could lead to polymeric mesh structures that more closely resemble the network structure shown in Fig. 10A. Porous polymers have a broad range of applications (*87*), and BPs could provide access to a pore structure that might be difficult to accomplish through other methods.

Inorganic photonic crystals from BP templates

Creating inorganic photonic crystals from BP templates is an unexplored direction. Inorganic photonic crystals are likely to be stable over a wider temperature range and more resistant to degradation than their organic counterparts. Synthesizing inorganic structures from organic templates is an area of intense research, and recent developments in the field could guide the fabrication of inorganic photonic crystals from BPs. Inorganic photonic crystals made of silica have been prepared starting from bio-templates (*88*, *89*) using a sol-gel method. Sequential infiltration synthesis has been used to prepare inorganic nanostructures from BCP templates (*85*, *90*, *91*). It remains to be seen if these templating techniques can be applied with success to BPs. Templating processes would require careful optimization of the chemistry and mechanical properties of BPs.

New BP symmetries

Electric fields have been used to create BP structures with new lattice symmetries (*92*). Reports of BPs with hexagonal (*93*) and tetragonal symmetry (*94*) date back to the 1980s. Recently, Lin and coworkers (*95*) applied repetitive electrical pulses to access orthorhombic and tetragonal BPs, and subsequently used photopolymerization to freeze these noncubic states. Reports of preparation of noncubic BPs have used electric fields. Identification of alternate methods of creating noncubic BPs could expand the range of BP lattice symmetries. The range of lattice symmetries that can be attained in liquid BPs determines the diversity of photonic materials that can be created from polymerization.

Compositional heterogeneity in BPs

BPs typically consist of multiple molecular species; however, the organization of different molecules in the unit cell is poorly understood. Techniques sensitive to nanoscale compositional fluctuations such as resonant soft x-ray scattering (*96*, *97*) and energy-filtered transmission electron microscopy (*98*, *99*) can be used to fill this gap in understanding. SEM measurements, like the one shown in Fig. 10B, wherein the unpolymerized regions of UV-cured BPs are washed out, indicate that spatial variations in composition exist. Quantifying spatial variations in chemical composition, in both polymerized and unpolymerized materials, is essential for understanding BP structure, which in turn is essential for using BPs as templates for material synthesis.

CONCLUSIONS

BPs are three-dimensional photonic crystals that form spontaneously through molecular self-assembly in a narrow temperature window between the cholesteric and isotropic phases. Low–molecular weight liquid BPs can be converted to polymeric states with retention of structure. The polymeric materials prepared through this route simultaneously exhibit mechanical robustness, stimuli responsiveness, and photonic crystallinity, a combination of properties that can be exploited for sensing, display, and camouflage applications. Advances in experiments have led to the development of several strategies to control lattice orientation, which is essential for achieving spatially uniform optical properties in BP-based materials. Computer simulations have evolved in parallel with experiments, paving the path for computational design of BP-based materials in the future. Developments in computer simulations could also allow for quantification of compositional and dynamic heterogeneity in BPs, which could have profound fundamental and technological implications.

REFERENCES AND NOTES

1. M. Mitov, Cholesteric liquid crystals with a broad light reflection band. *Adv. Mater.* **24**, 6260–6276 (2012).
2. H. K. Bisoyi, Q. Li, Liquid crystals: Versatile self-organized smart soft materials. *Chem. Rev.* **122**, 4887–4926 (2021).
3. V. Sharma, M. Crne, J. O. Park, M. Srinivasarao, Structural origin of circularly polarized iridescence in jeweled beetles. *Science* **325**, 449–451 (2009).
4. L. Wang, A. M. Urbas, Q. Li, Nature-inspired emerging chiral liquid crystal nanostructures: From molecular self-assembly to DNA mesophase and nanocolloids. *Adv. Mater.* **32**, 1801335 (2020).
5. A. D. Rey, Liquid crystal models of biological materials and processes. *Soft Matter* **6**, 3402–3429 (2010).

6. E. Bukusoglu, X. Wang, J. A. Martinez-Gonzalez, J. J. de Pablo, N. L. Abbott, Stimuli-responsive cubosomes formed from blue phase liquid crystals. *Adv. Mater.* **27**, 6892–6898 (2015).
7. E. Oton, E. Netter, T. Nakano, F. Inoue, Monodomain blue phase liquid crystal layers for phase modulation. *Sci. Rep.* **7**, 44575 (2017).
8. E. Bukusoglu, M. Bedolla Pantoja, P. C. Mushenheim, X. Wang, N. L. Abbott, Design of responsive and active (soft) materials using liquid crystals. *Annu. Rev. Chem. Biomol. Eng.* **7**, 163–196 (2016).
9. S. S. Gandhi, L.-C. Chien, Unraveling the mystery of the blue fog: Structure, properties, and applications of amorphous blue phase III. *Adv. Mater.* **29**, 1704296 (2017).
10. O. Henrich, K. Stratford, M. E. Cates, D. Marenduzzo, Structure of blue phase III of cholesteric liquid crystals. *Phys. Rev. Lett.* **106**, 107801 (2011).
11. A. N. Bogdanov, C. Panagopoulos, Physical foundations and basic properties of magnetic skyrmions. *Nat. Rev. Phys.* **2**, 492–498 (2020).
12. J. Pišljar, S. Ghosh, S. Turlapati, N. V. S. Rao, M. Škarabot, A. Mertelj, A. Petelin, A. Nych, M. Marinčič, A. Pusovnik, Blue phase III: Topological fluid of skyrmions. *Phys. Rev. X* **12**, 11003 (2022).
13. D. K. Yang, P. P. Crooker, Chiral-racemic phase diagrams of blue-phase liquid crystals. *Phys. Rev. A* **35**, 4419–4423 (1987).
14. J. Yang, J. Liu, B. Guan, W. He, Z. Yang, J. Wang, T. Ikeda, L. Jiang, Fabrication and photonic applications of large-domain blue phase films. *J. Mater. Chem. C.* **7**, 9460–9466 (2019).
15. G. Von Freymann, A. Ledermann, M. Thiel, I. Staude, S. Essig, K. Busch, M. Wegener, Three-dimensional nanostructures for photonics. *Adv. Funct. Mater.* **20**, 1038–1052 (2010).
16. M. Campbell, D. N. Sharp, M. T. Harrison, R. G. Denning, A. J. Turberfield, Fabrication of photonic crystals for the visible spectrum by holographic lithography. *Nature* **404**, 53–56 (2000).
17. P. Nayek, H. Jeong, H. R. Park, S.-W. Kang, S. H. Lee, H. S. Park, H. J. Lee, H. S. Kim, Tailoring monodomain in blue phase liquid crystal by surface pinning effect. *Appl. Phys. Express.* **5**, 051701 (2012).
18. H. Lee, H.-J. Park, O.-J. Kwon, S. J. Yun, J. H. Park, S. Hong, S.-T. Shin, 11.1: Invited Paper: The world's first blue phase liquid crystal display. *SID Symp. Dig. Tech. Pap.* **42**, 121–124 (2011).
19. Y. Chen, S.-T. Wu, Recent advances on polymer-stabilized blue phase liquid crystal materials and devices. *J. Appl. Polym. Sci.* **131**, (2014).
20. M. D. A. Rahman, S. M. Said, S. Balamurugan, Blue phase liquid crystal: Strategies for phase stabilization and device development. *Sci. Technol. Adv. Mater.* **16**, 033501 (2015).
21. W. Hu, J. Sun, Q. Wang, L. Zhang, X. Yuan, F. Chen, K. Li, Z. Miao, D. Yang, H. Yu, Humidity-responsive blue phase liquid-crystalline film with reconfigurable and tailored visual signals. *Adv. Funct. Mater.* **30**, 2004610 (2020).
22. Y. Yang, Y.-K. Kim, X. Wang, M. Tsuei, N. L. Abbott, Structural and optical response of polymer-stabilized blue phase liquid crystal films to volatile organic compounds. *ACS Appl. Mater. Interfaces* **12**, 42099–42108 (2020).
23. F. Castles, F. V. Day, S. M. Morris, D. H. Ko, D. J. Gardiner, M. M. Qasim, S. Nosheen, P. J. W. Hands, S. S. Choi, R. H. Friend, H. J. Coles, Blue-phase templated fabrication of three-dimensional nanostructures for photonic applications. *Nat. Mater.* **11**, 599–603 (2012).
24. W. Cao, A. Munoz, P. Palffy-Muhoray, B. Taheri, Lasing in a three-dimensional photonic crystal of the liquid crystal blue phase II. *Nat. Mater.* **1**, 111–113 (2002).
25. S. Yokoyama, S. Mashiko, H. Kikuchi, K. Uchida, T. Nagamura, Laser emission from a polymer-stabilized liquid-crystalline blue phase. *Adv. Mater.* **18**, 48–51 (2006).
26. M. Wang, C. Zou, J. Sun, L. Zhang, L. Wang, J. Xiao, F. Li, P. Song, H. Yang, Asymmetric tunable photonic bandgaps in self-organized 3D nanostructure of polymer-stabilized blue phase I modulated by voltage polarity. *Adv. Funct. Mater.* **27**, 1702261 (2017).
27. S.-T. Hur, B. R. Lee, M.-J. Gim, K.-W. Park, M. H. Song, S.-W. Choi, Liquid-crystalline blue phase laser with widely tunable wavelength. *Adv. Mater.* **25**, 3002–3006 (2013).
28. H. Choi, H. Higuchi, H. Kikuchi, Electrooptic response of liquid crystalline blue phases with different chiral pitches. *Soft Matter* **7**, 4252–4256 (2011).
29. T. A. Kumar, K. V. Le, S. Aya, S. Kang, F. Araoka, K. Ishikawa, S. Dhara, H. Takezoe, Anchoring transition in a nematic liquid crystal doped with chiral agents. *Phase Transit.* **85**, 888–899 (2012).
30. W. He, G. Pan, Z. Yang, D. Zhao, G. Niu, W. Huang, X. Yuan, J. Guo, H. Cao, H. Yang, Wide blue phase range in a hydrogen-bonded self-assembled complex of chiral fluoro-substituted benzoic acid and pyridine derivative. *Adv. Mater.* **21**, 2050–2053 (2009).
31. H. J. Coles, M. N. Pivnenko, Liquid crystal 'blue phases' with a wide temperature range. *Nature* **436**, 997–1000 (2005).
32. W. Hu, L. Wang, M. Wang, T. Zhong, Q. Wang, L. Zhang, F. Chen, K. Li, Z. Miao, D. Yang, Ultrastable liquid crystalline blue phase from molecular synergistic self-assembly. *Nat. Commun.* **12**, 1440 (2021).
33. Z. Zheng, D. Shen, P. Huang, Wide blue phase range of chiral nematic liquid crystal doped with bent-shaped molecules. *New J. Phys.* **12**, 113018 (2010).
34. W.-Q. Yang, G.-Q. Cai, Z. Liu, X.-Q. Wang, W. Feng, Y. Feng, D. Shen, Z. Zheng, Room temperature stable helical blue phase enabled by a photo-polymerizable bent-shaped material. *J. Mater. Chem. C.* **5**, 690–696 (2017).
35. J.-i. Fukuda, Stabilization of a blue phase by a guest component: An approach based on a Landau–de Gennes theory. *Phys. Rev. E. Stat. Nonlin. Soft Matter Phys.* **82**, 061702 (2010).
36. M. A. Gharbi, S. Manet, J. Lhermitte, S. Brown, J. Milette, V. Toader, M. Sutton, L. Reven, Reversible nanoparticle cubic lattices in blue phase liquid crystals. *ACS Nano* **10**, 3410–3415 (2016).
37. V. Sridurai, M. Mathews, C. V. Yelamaggad, G. G. Nair, Electrically tunable soft photonic gel formed by blue phase liquid crystal for switchable color-reflecting mirror. *ACS Appl. Mater. Interfaces* **9**, 39569–39575 (2017).
38. D. J. Broer, On the history of reactive mesogens: Interview with Dirk J. Broer. *Adv. Mater.* **32**, 1905144 (2020).
39. D. J. Broer, H. Finkelmann, K. Kondo, In-situ photopolymerization of an oriented liquid-crystalline acrylate. *Die Makromol. Chem.* **189**, 185–194 (1988).
40. K. R. Schlafmann, T. J. White, Retention and deformation of the blue phases in liquid crystalline elastomers. *Nat. Commun.* **12**, 4916 (2021).
41. E. Kemiklioglu, L.-C. Chien, Polymer-encapsulated blue phase liquid crystal droplets. *Appl. Phys. Express.* **7**, 091701 (2014).
42. M. Sadati, J. A. Martinez-Gonzalez, Y. Zhou, N. T. Qazvini, K. Kurtenbach, X. Li, E. Bukusoglu, R. Zhang, N. L. Abbott, J. P. Hernandez-Ortiz, Prolate and oblate chiral liquid crystal spheroids. *Sci. Adv.* **6**, eaba6728 (2020).
43. J. A. Martinez-Gonzalez, Y. Zhou, M. Rahimi, E. Bukusoglu, N. L. Abbott, J. J. de Pablo, Blue-phase liquid crystal droplets. *Proc. Natl. Acad. Sci. U.S.A.* **112**, 13195–13200 (2015).
44. F. Castles, S. M. Morris, J. M. C. Hung, M. M. Qasim, A. D. Wright, S. Nosheen, S. S. Choi, B. I. Outram, S. J. Elston, C. Burgess, L. Hill, T. D. Wilkinson, H. J. Coles, Stretchable liquid-crystal blue-phase gels. *Nat. Mater.* **13**, 817–821 (2014).
45. C.-W. Chen, C.-T. Hou, C.-C. Li, H.-C. Jau, C.-T. Wang, C.-L. Hong, D.-Y. Guo, C.-Y. Wang, S.-P. Chiang, T. J. Bunning, I.-C. Khoo, T.-H. Lin, Large three-dimensional photonic crystals based on monocrystalline liquid crystal blue phases. *Nat. Commun.* **8**, 727 (2017).
46. S.-Y. Jo, S.-W. Jeon, B.-C. Kim, J.-H. Bae, F. Araoka, S.-W. Choi, Polymer stabilization of liquid-crystal blue phase II toward photonic crystals. *ACS Appl. Mater. Interfaces* **9**, 8941–8947 (2017).
47. H. Kikuchi, M. Yokota, Y. Hisakado, H. Yang, T. Kajiyama, Polymer-stabilized liquid crystal blue phases. *Nat. Mater.* **1**, 64–68 (2002).
48. H. Kim, J. Choi, K. K. Kim, P. Won, S. Hong, S. H. Ko, Biomimetic chameleon soft robot with artificial crypsis and disruptive coloration skin. *Nat. Commun.* **12**, 4658 (2021).
49. J. Yan, S.-T. Wu, K.-L. Cheng, J.-W. Shiu, A full-color reflective display using polymer-stabilized blue phase liquid crystal. *Appl. Phys. Lett.* **102**, 81102 (2013).
50. Z.-G. Zheng, C.-L. Yuan, W. Hu, H. K. Bisoyi, M.-J. Tang, Z. Liu, P.-Z. Sun, W.-Q. Yang, X.-Q. Wang, D. Shen, Y. Li, F. Ye, Y.-Q. Lu, G. Li, Q. Li, Light-patterned crystallographic direction of a self-organized 3D soft photonic crystal. *Adv. Mater.* **29**, 1703165 (2017).
51. J. A. Martinez-González, X. Li, M. Sadati, Y. Zhou, R. Zhang, P. F. Nealey, J. J. de Pablo, Directed self-assembly of liquid crystalline blue-phases into ideal single-crystals. *Nat. Commun.* **8**, 15854 (2017).
52. K. Kim, S. Kim, S.-Y. Jo, S.-W. Choi, A monodomain-like liquid-crystalline simple cubic blue phase II. *J. Inf. Disp.* **16**, 155–160 (2015).
53. J. Czochralski, A new method for the measurement of the crystallization rate of metals. *Z. Phys. Chem.* **92**, 219–221 (1918).
54. P. Tomaszewski, Jan Czochralski—Father of the Czochralski method. *J. Cryst. Growth* **236**, 1–4 (2002).
55. R. Uecker, The historical development of the Czochralski method. *J. Cryst. Growth* **401**, 7–24 (2014).
56. Y. Chen, S.-T. Wu, Electric field-induced monodomain blue phase liquid crystals. *Appl. Phys. Lett.* **102**, 171110 (2013).
57. X. Li, J. A. Martinez-González, J. P. Hernández-Ortiz, A. Ramirez-Hernández, Y. Zhou, M. Sadati, R. Zhang, P. F. Nealey, J. J. De Pablo, Mesoscale martensitic transformation in single crystals of topological defects. *Proc. Natl. Acad. Sci. U.S.A.* **114**, 10011–10016 (2017).
58. X. Li, J. A. Martínez-González, K. Park, C. Yu, Y. Zhou, J. J. de Pablo, P. F. Nealey, Perfection in nucleation and growth of blue-phase single crystals: Small free-energy required to self-assemble at specific lattice orientation. *ACS Appl. Mater. Interfaces* **11**, 9487–9495 (2019).
59. X. Li, J. C. Armas-Perez, J. A. Martinez-Gonzalez, X. Liu, H. Xie, C. Bishop, J. P. Hernandez-Ortiz, R. Zhang, J. J. De Pablo, P. F. Nealey, Directed self-assembly of nematic liquid crystals on chemically patterned surfaces: Morphological states and transitions. *Soft Matter* **12**, 8595–8605 (2016).
60. X. Li, T. Yanagimachi, C. Bishop, C. Smith, M. Dolejsi, H. Xie, K. Kurihara, P. F. Nealey, Engineering the anchoring behavior of nematic liquid crystals on a solid surface by varying the density of liquid crystalline polymer brushes. *Soft Matter* **14**, 7569–7577 (2018).

61. B. Bläsi, N. Tucher, O. Höhn, V. Kübler, T. Kroyer, C. Wellens, H. Hauser, Large area patterning using interference and nanoimprint lithography, in *Micro-Optics 2016* (SPIE, 2016), vol. 9888, p. 98880H.
62. X. Xu, J. Wang, Y. Liu, D. Luo, Large-scale single-crystal blue phase through holography lithography. *Adv. Photon. Nexus* **2**, 26004 (2023).
63. X. Li, J. A. Martinez-Gonzalez, J. J. de Pablo, P. Nealey, Thickness dependence of forming single crystal by liquid-crystalline blue phase on chemically patterned surface, in *Emerging Liquid Crystal Technologies XIII* (SPIE, 2018), vol. 10555, pp. 136–144.
64. X. Chen, P. R. Delgadillo, Z. Jiang, G. S. W. Craig, R. Gronheid, P. F. Nealey, Defect annihilation in the directed self-assembly of block copolymers in films with increasing thickness. *Macromolecules* **52**, 7798–7805 (2019).
65. A. M. Welander, G. S. W. Craig, Y. Tada, H. Yoshida, P. F. Nealey, Directed assembly of block copolymers in thin to thick films. *Macromolecules* **46**, 3915–3921 (2013).
66. M. Ravnik, S. Žumer, Landau–de Gennes modelling of nematic liquid crystal colloids. *Liq. Cryst.* **36**, 1201–1214 (2009).
67. J.-B. Fournier, P. Galatola, Modeling planar degenerate wetting and anchoring in nematic liquid crystals. *EPL* **72**, 403–409 (2005).
68. G. P. Alexander, J. M. Yeomans, Numerical results for the blue phases. *Liq. Cryst.* **36**, 1215–1227 (2009).
69. A. Dupuis, D. Marenduzzo, J. M. Yeomans, Numerical calculations of the phase diagram of cubic blue phases in cholesteric liquid crystals. *Phys. Rev. E* **71**, 011703 (2005).
70. T. Emeršič, K. Bagchi, J. A. Martinez-González, X. Li, J. J. de Pablo, P. F. Nealey, A generalizable approach to direct the self-assembly of functional blue-phase liquid crystals. *Adv. Funct. Mater.* **32**, 2202721 (2022).
71. M. Ravnik, G. P. Alexander, J. M. Yeomans, S. Žumer, Three-dimensional colloidal crystals in liquid crystalline blue phases. *Proc. Natl. Acad. Sci. U.S.A.* **108**, 5188–5192 (2011).
72. O. Wiese, D. Marenduzzo, O. Henrich, Microfluidic flow of cholesteric liquid crystals. *Soft Matter* **12**, 9223–9237 (2016).
73. J.-i. Fukuda, M. Yoneya, H. Yokoyama, Simulation of cholesteric blue phases using a Landau–de Gennes theory: Effect of an applied electric field. *Phys. Rev. E* **80**, 031706 (2009).
74. A. Yu, E. M. Y. Lee, J. A. G. Briggs, B. K. Ganser-Pornillos, O. Pornillos, G. A. Voth, Strain and rupture of HIV-1 capsids during uncoating. *Proc. Natl. Acad. Sci. U.S.A.* **119**, e2117781119 (2022).
75. A. P. Draude, T. Y. Kalavalapalli, M. Iliut, B. McConnell, I. Dierking, Stabilization of liquid crystal blue phases by carbon nanoparticles of varying dimensionality. *Nanoscale Adv.* **2**, 2404–2409 (2020).
76. W.-L. He, W.-K. Zhang, H. Xu, L.-H. Li, Z. Yang, H. Cao, D. Wang, Z.-G. Zheng, H. Yang, Preparation and optical properties of Fe_3O_4 nanoparticles-doped blue phase liquid crystal. *Phys. Chem. Chem. Phys.* **18**, 29028–29032 (2016).
77. L. Wang, W. He, X. Xiao, M. Wang, M. Wang, P. Yang, Z. Zhou, H. Yang, H. Yu, Y. Lu, Low voltage and hysteresis-free blue phase liquid crystal dispersed by ferroelectric nanoparticles. *J. Mater. Chem.* **22**, 19629–19633 (2012).
78. J. Tang, F. Liu, M. Lu, D. Zhao, InP/ZnS quantum dots doped blue phase liquid crystal with wide temperature range and low driving voltage. *Sci. Rep.* **10**, 18067 (2020).
79. M. Stimulak, M. Ravnik, Tunable photonic crystals with partial bandgaps from blue phase colloidal crystals and dielectric-doped blue phases. *Soft Matter* **10**, 6339–6346 (2014).
80. S. Yadav, P. Malik, P. Malik, CdTe quantum dot-polymer stabilized blue phase liquid crystal nanocomposite with wide blue phase and improved electro-optical responses. *Opt. Mater.* **137**, 113608 (2023).
81. S. K. Kumar, B. C. Benicewicz, R. A. Vaia, K. I. Winey, 50th anniversary perspective: Are polymer nanocomposites practical for applications? *Macromolecules* **50**, 714–731 (2017).
82. S. K. Kumar, R. Krishnamoorti, Nanocomposites: Structure, phase behavior, and properties. *Annu. Rev. Chem. Biomol. Eng.* **1**, 37–58 (2010).
83. L. Wang, W. He, Q. Wang, M. Yu, X. Xiao, Y. Zhang, M. Ellahi, D. Zhao, H. Yang, L. Guo, Polymer-stabilized nanoparticle-enriched blue phase liquid crystals. *J. Mater. Chem. C* **1**, 6526–6531 (2013).
84. X. Feng, M. E. Tousley, M. G. Cowan, B. R. Wiesenauer, S. Nejati, Y. Choo, R. D. Noble, M. Elimelech, D. L. Gin, C. O. Osuji, Scalable fabrication of polymer membranes with vertically aligned 1 nm pores by magnetic field directed self-assembly. *ACS Nano* **8**, 11977–11986 (2014).
85. C. Zhou, T. Segal-Peretz, M. E. Oruc, H. S. Suh, G. Wu, P. F. Nealey, Fabrication of nanoporous alumina ultrafiltration membrane with tunable pore size using block copolymer templates. *Adv. Funct. Mater.* **27**, 1701756 (2017).
86. H. Kikuchi, S. Izena, H. Higuchi, Y. Okumura, K. Higashiguchi, A giant polymer lattice in a polymer-stabilized blue phase liquid crystal. *Soft Matter* **11**, 4572–4575 (2015).
87. D. Wu, F. Xu, B. Sun, R. Fu, H. He, K. Matyjaszewski, Design and preparation of porous polymers. *Chem. Rev.* **112**, 3959–4015 (2012).
88. J. W. Galusha, L. R. Richey, M. R. Jorgensen, J. S. Gardner, M. H. Bartl, Study of natural photonic crystals in beetle scales and their conversion into inorganic structures *via* a sol–gel bio-templating route. *J. Mater. Chem.* **20**, 1277–1284 (2010).
89. C. Mille, E. C. Tyrode, R. W. Corkery, Inorganic chiral 3-D photonic crystals with bicontinuous gyroid structure replicated from butterfly wing scales. *Chem. Commun.* **47**, 9873–9875 (2011).
90. Q. Peng, Y.-C. Tseng, S. B. Darling, J. W. Elam, A route to nanoscopic materials via sequential infiltration synthesis on block copolymer templates. *ACS Nano* **5**, 4600–4606 (2011).
91. Y.-C. Tseng, Q. Peng, L. E. Ocola, J. W. Elam, S. B. Darling, Enhanced block copolymer lithography using sequential infiltration synthesis. *J. Phys. Chem. C* **115**, 17725–17729 (2011).
92. H.-S. Kitzerow, The effect of electric fields on blue phases. *Mol. Cryst. Liq. Cryst.* **202**, 51–83 (1991).
93. P. Pieranski, P. E. Cladis, R. Barbet-Massin, Experimental evidence for a hexagonal blue phase. *J. Phys. Lett.* **46**, 973–977 (1985).
94. P. Pieranski, P. E. Cladis, Field-induced tetragonal blue phase (BPX). *Phys. Rev. A* **35**, 355–364 (1987).
95. D.-Y. Guo, C.-W. Chen, C.-C. Li, H.-C. Jau, K.-H. Lin, T.-M. Feng, C.-T. Wang, T. J. Bunning, I. C. Khoo, T.-H. Lin, Reconfiguration of three-dimensional liquid-crystalline photonic crystals by electrostriction. *Nat. Mater.* **19**, 94–101 (2020).
96. F. Liu, M. A. Brady, C. Wang, Resonant soft X-ray scattering for polymer materials. *Eur. Polym. J.* **81**, 555–568 (2016).
97. B. A. Collins, E. Gann, Resonant soft X-ray scattering in polymer science. *J. Polym. Sci* **60**, 1199–1243 (2022).
98. L. F. Drummy, R. J. Davis, D. L. Moore, M. Durstock, R. A. Vaia, J. W. P. Hsu, Molecular-scale and nanoscale morphology of P3HT: PCBM bulk heterojunctions: Energy-filtered TEM and low-dose HREM. *Chem. Mater.* **23**, 907–912 (2011).
99. M. A. Brady, G. M. Su, M. L. Chabinyc, Recent progress in the morphology of bulk heterojunction photovoltaics. *Soft Matter* **7**, 11065–11077 (2011).

Acknowledgments

Funding: We gratefully acknowledge support from the U.S. Department of Energy (DOE), Basic Energy Sciences, Materials Sciences and Engineering Division. **Author contributions:** K.B. and P.F.N. conceived the topic of the review. K.B., T.E., and J.A.M.-G. wrote the manuscript. P.F.N., J.A.M.-G., and J.J.d.P. edited and reviewed the paper before submission. All the authors contributed to discussions of the manuscript. **Competing interests:** The authors declare that they have no competing interests. **Data and materials availability:** All data needed to evaluate the conclusions in the paper are present in the paper.

Submitted 23 March 2023
Accepted 27 June 2023
Published 26 July 2023
10.1126/sciadv.adh9393

ScienceAdvances

Functional soft materials from blue phase liquid crystals

Kushal Bagchi, Tadej Emeri, Jos A. Martnez-Gonzlez, Juan J. de Pablo, and Paul F. Nealey

Sci. Adv., **9** (30), eadh9393.
DOI: 10.1126/sciadv.adh9393